

The non-peculiar velocity dispersion profile of the stellar system ω Centauri^{*}

A. Sollima¹†, M. Bellazzini², R. L. Smart³, M. Correnti⁴, E. Pancino²,
F. R. Ferraro⁴ and D. Romano⁴

¹ *Instituto de Astrofísica de Canarias, c/vía Lactea s/n, San Cristobal de La Laguna, 38205, Spain*

² *INAF Osservatorio Astronomico di Bologna, via Ranzani 1, Bologna, 40127, Italy*

³ *INAF, Osservatorio Astronomico di Torino, via Osservatorio 20, 10025 Pino Torinese, Italy*

⁴ *Dipartimento di Astronomia, Università di Bologna, via Ranzani 1, Bologna, 40127, Italy*

Accepted 2009 February 11. Received 2009 February 11; in original form 2009 February 11

ABSTRACT

We present the results of a survey of radial velocities over a wide region extending from $r \simeq 10'$ out to $r \simeq 80'$ (~ 1.5 tidal radii) within the massive star cluster ω Centauri. The survey was performed with FLAMES@VLT, to study the velocity dispersion profile in the outer regions of this stellar system. We derived accurate radial velocities for a sample of 2557 newly observed stars, identifying 318 bona-fide cluster red giants. Merging our data with those provided by Pancino et al. (2007), we assembled a final homogeneous sample of 946 cluster members that allowed us to trace the velocity dispersion profile from the center out to $r \sim 32$ arcmin. The velocity dispersion appears to decrease monotonically over this range, from a central value of $\sigma_v \sim 17.2 \text{ Km s}^{-1}$ down to a minimum value of $\sigma_v \sim 5.2 \text{ Km s}^{-1}$. The observed surface brightness profile, rotation curve, velocity dispersion profile and ellipticity profile are simultaneously well reproduced by a simple dynamical model in which mass follows light, within the classical Newtonian theory of gravitation. The comparison with an N-body model of the evolution of a system mimicking ω Cen during the last 10 orbits into the Galactic potential suggests that (a) the rotation of stars lying in the inner $\simeq 20'$ of the clusters is not due to the effects of the tidal field of the Milky Way, as hypothesized by other authors, and (b) the overall observational scenario is still compatible with the possibility that the outer regions of the cluster are subject to some tidal stirring.

Key words: stars: kinematics – stars: Population II – globular clusters : individual: ω Centauri – techniques: radial velocities

1 INTRODUCTION

ω Centauri is the most massive and luminous globular cluster (GC) of the Milky Way ($M \sim 2.5 \cdot 10^6 M_\odot$; van de Ven et al. 2006). It is the only known Galactic GC which shows clear star-to-star variations in the abundance of iron-peak elements (Freeman & Rodgers 1975; Norris, Freeman & Mighell 1996) and indication exists for possible helium abundance variation among its stellar populations (Norris 2004; Piotto et al. 2005). Together with a few other clusters (like M54 and NGC2419, for example), ω Cen fall well above the sharp upper envelope of the main distribution of GCs on

the size-luminosity plane (Mackey & van den Bergh 2005; Federici et al. 2007). These (and other) evidences suggest that ω Cen could be not a "genuine" GC but more likely the nuclear remnant of a dwarf galaxy that merged in the past with the Milky Way (Freeman 1993; see Bellazzini et al. 2008 for a discussion of the analogy with the case of M54 within the disrupting Sgr dwarf galaxy).

From the dynamical point of view, ω Cen is one of the most flattened among Galactic GCs (Meylan 1987). The flattening is generally interpreted as due to the observed rotation, as the variations of ellipticity with distance from the cluster center correlates with the amplitude of the rotation curve (Merritt, Meylan, & Mayor 1997; Meylan & Mayor 1986). Merritt et al.(1997) found that ω Cen can be well described as an isotropic oblate rotator in which the mass is distributed as the light. In a recent study Van de Ven et al. (2006) modelled ω Cen with an axisymmetric implementation of Schwarzschild's orbit superposition method.

* Based on FORS observations collected with the Very Large Telescope at the European Southern Observatory, Cerro Paranal, Chile, within the observing programs 071.D-0217A and 081.D-0255A.

† E-mail: asollima@iac.es

They found that the system is close to isotropic inside a radius of about 10 arcmin and becomes increasingly tangentially anisotropic in the outer region, which displays significant mean rotation. These authors suggested that this phase-space structure could be caused by the effects of the tidal field of the Milky Way, as kinematical gradients are a typical outcome of tidal stresses (see Muñoz et al. 2008 and references therein).

A number of studies on the kinematics of the cluster have been performed in the recent past (Meylan et al. 1995; Mayor et al. 1997; Norris et al. 1997; Reijns et al. 2006; Van de Ven et al. 2006), particularly focused on the innermost $r \lesssim 20'$ region. Recently, Scarpa, Marconi & Gilmozzi (2003) measured the velocity dispersion profile of ω Cen at larger distances ($20' < r < 28'$) using UVES spectra of 75 candidate cluster members. They found that the velocity dispersion profile remains constant at large radii rather than decrease monotonically, as expected for systems in which mass follows light. These authors suggested that this behaviour could be due to a breakdown of Newton's law in the weak acceleration regime, as proposed in the popular Modified Newtonian Dynamics framework (MOND, Milgrom 1983, 2008). However, it has been noted that actually this cannot be the case, as a flat velocity profile at large radii is predicted by MOND only for clusters in the deepest MOND regime, i.e. where both the internal acceleration and that due to the gravitational field of the Milky Way are significantly lower than the MOND scale acceleration, $a_0 \simeq 1.2 \times 10^{-8}$ cm/s² (Baumgardt, Grebel & Kroupa 2005; Moffat & Toth 2008). On the contrary, at the position of ω Cen the external acceleration due to the Milky Way is $\gtrsim a_0$. In this regime, the predictions of MOND are similar to the Newtonian behaviour (see also Moffat & Toth 2008; Haghi et al. 2009).

Nevertheless, a flat velocity dispersion profile over a large radial range would be incompatible with a mass-follow-light model (Gilmore et al. 2007) and may suggest the presence of a halo of Dark matter (DM) embedding the star cluster and driving the kinematics of the stars in the outer regions (Carraro & Lia 2000; Mashchenko & Sills 2005). In any case the available evidences are not sufficient to support the case of DM: as McLaughlin & Meylan (2003) demonstrated, Scarpa et al.'s data could be well described by simple, self-consistent dynamical models without the need of MOND and/or dark matter. A larger kinematic survey in the region $r > 20'$ is overdue to assess the behaviour of the dispersion profile in this range.

A controversial issue is also represented by the possible presence of signatures of tidal effects in the outskirts of this stellar system. If the present-day cluster is just the nuclear remnant of a larger system, it is reasonable to expect some observable overdensity of stripped stars in the surroundings, if the latest phase of disruption occurred in the recent past (up to a few orbital period ago; see Combes, Leon & Meylan 1999; Dinescu (2002); Tsuchiya, Korchagin & Dinescu 2004; Mizutani, Chiba & Sakamoto 2003; Ideta & Makino 2004; Bekki & Freeman 2003). Leon, Meylan & Combes (2000) studied the 2-D structures of the distribution of stars around ω Cen from $5.5^\circ \times 5.5^\circ$ photographic films obtained with the ESO Schmidt telescope. This analysis evidenced the presence of a pair of tidal tails approximately oriented in the direction of the Galactic center, in projection. This result has been questioned by Law et al. (2003) who

found that *a)* Leon's et al. tidal tails were strongly correlated with inhomogeneities in the reddening distribution and *b)* no extra-tidal component can be detected using the homogeneous near-infrared photometry of the 2MASS survey. In a recent dedicated survey, Da Costa & Coleman (2008) derived the radial velocities (with an accuracy of ~ 10 Km s⁻¹) of 4105 stars located on a wide region out to a distance of 2 tidal radii from the cluster center. They estimated that less than 0.7% of the total cluster mass is comprised between 1 and 2 tidal radii, implying that the stripping process on the progenitor (if any) must have been largely completed at early epochs.

In this paper we present the results of a survey of radial velocities in ω Cen performed with FLAMES@VLT, focused on the radial range $10' \lesssim r \lesssim 30'$ and aimed at the assessment of the kinematical properties in the outskirts of the cluster. The new dataset, combined with the homogeneous sample of Pancino et al. (2007), allowed us to derive a robust velocity dispersion profile from the center to a distance of $32'$ with an accuracy ≤ 1 Km s⁻¹. In §2 we describe the observations and the data reduction techniques. In §3 we present the metallicity and the velocity distributions. Section 4 is devoted to the description of the method used to derive the velocity dispersion profile of ω Cen. In §5 we compare the observed kinematics of this stellar system with a set of dynamical models and N-body simulations. Section 6 is devoted to the analysis of the sample of stars located in the outer region of ω Cen. Finally, we summarize and discuss our results in §7.

2 OBSERVATIONS AND DATA REDUCTION

The analysis presented here is based on two spectroscopic datasets: *i)* the *inner sample*: constituted of a sample of ~ 700 red giants selected from the photometry by Pancino et al. (2000) in the magnitude range $13 < B < 16$ lying within $15'$ from the cluster center and presented in Pancino et al. (2007; hereafter P07), and *ii)* the *outer sample*: constituted of a sample of 2557 red giants selected from the 2MASS catalog (Skrutskie et al. 2006) between $6.0 < K < 13.0$, observed in 28 pointings at distances $10' < r < 80'$ from the cluster center (see Figure 1).

At $r \sim 20'$ from the cluster center, the surface brightness is already $\mu_V > 22.0$ mag/arcsec², implying that Red Giant Branch (RGB) stars of ω Cen should be relatively rare and indeed not numerous enough to fill all the fibers of a single FLAMES plate. To achieve the maximum efficiency in selecting cluster members for the *outer sample* we gave the highest priority for fiber allocation to stars (a) lying within a selection box in color-magnitude diagram broadly enclosing the cluster RGB (see Fig. 5), defined from the accurate infrared photometry by Sollima et al. (2004), and (b) with UCAC2 (Zacharias et al. 2004) proper motions differing by less than ± 8 mas yr⁻¹ from the bulk proper motion of the cluster, as determined by van Leeuwen et al. (2000). These "a priori" criteria allowed to select some hundreds high-confidence target stars. The remaining fibers were positioned on other stars selected from the 2MASS catalog in the same magnitude range, as shown in Fig. 5, below.

Observations have been done with FLAMES (Pasquini et al. 2002) at the ESO VLT in Paranal, Chile, between 2003

May 22 and 28 (*inner sample*, P07) and between 2008 July 13 and August 20 (*outer sample*). In both cases, FLAMES has been used in GIRAFFE mode, using the high-resolution ($R \sim 22,500$) grating HR13 (6120-6395 Å) and reaching a signal-to-noise ratio of 50 – 300 $pixel^{-1}$, depending on the star magnitude. The *inner sample* has been already used by P07 to study the rotation pattern of the stellar populations of ω Cen. The data reduction and calibration procedure is very similar to that adopted here for the *outer sample* (see below), and is described in detail in P07.

The *outer sample* data have been reduced with the GIRAFFE BLDRS (Base-Line Data Reduction Software) 4 which includes cosmic-ray removal, bias subtraction, flat-field correction, wavelength calibration, and pixel resampling. Sixteen fibers have been dedicated to sky observations in each exposure. An average sky spectrum has been obtained and subtracted from the object spectra by taking into account the different fiber transmission. The spectra have been then continuum-normalized and corrected for telluric absorption bands with IRAF. The spectra of three program stars are shown in Figure 2 to illustrate the quality of our data.

Radial velocities have been derived through Fourier cross-correlation, using the *fxcor* task in the radial velocity IRAF package. The spectrum of each object has been correlated with a high signal-to-noise template spectrum of the Geneva radial velocity standard star HD42807, retrieved from the ELODIE archive (Moultaka et al. 2004). All spectra have been corrected for heliocentric velocity¹. The average error on the derived radial velocity is $\sigma_v \sim 0.5 \text{ Km s}^{-1}$. Nine stars are in common between the *inner* and the *outer* samples: the average difference in radial velocity is $\Delta v_r = -0.09 \pm 0.16$, fully consistent with no systematic shift between the two samples. Star by star comparisons with other datasets are also very satisfying. The average radial velocity difference of the 278 stars in common with Reijns et al. (2006) is $\Delta v_r = 1.48 \pm 1.76$, while for the 36 stars in common with Johnson et al. (2008) is $\Delta v_r = 1.62 \pm 1.47$, i.e., consistent with null difference within the uncertainties (Reijns et al. velocities were derived from spectra of resolution $8500 < R < 17000$; the resolution of Johnsons et al. spectra was $R=13000$; in both cases the typical uncertainty is $\sim 1.5 \text{ Km s}^{-1}$).

In addition, metallicities have been also derived for the *outer sample* stars. A set of 15 iron lines has been selected from the database of Kurucz & Bell (1995) in the spectral range covered by our spectra. These lines have been identified, whenever possible, on each spectrum and have been fitted with Gaussian functions. The integral of the difference between the continuum and the line profile provided the equivalent width (EW) of each line. The abundance analysis has been performed using the latest version of the Kurucz (1979) model atmospheres and the MOOG line analysis code (Snedden 1973) to compute LTE abundances from individual EWs. The abundance has been derived from the model that best reproduced the observed EWs, for assumed values of temperature, gravity, and microturbulence velocity. Temperatures have been derived from J-K colors adopting the color-

¹ The derived radial velocities of the *outer sample* stars are available in electronic form at the CDS (<http://cdsweb.u-strasbg.fr/>).

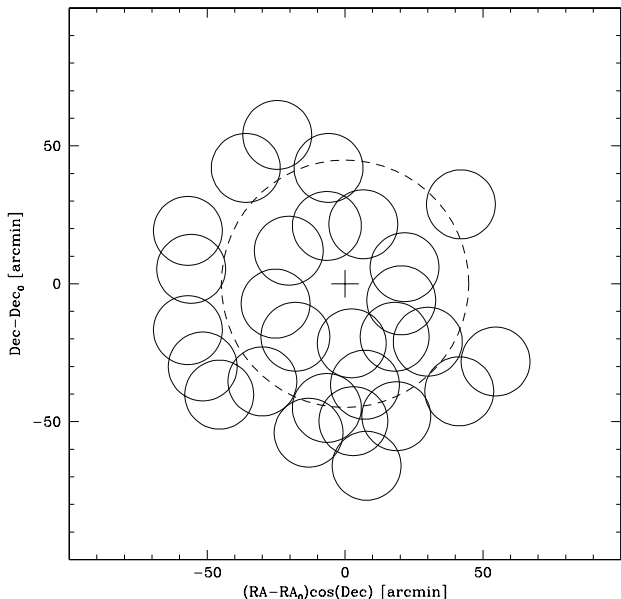


Figure 1. Map of the region sampled by the FLAMES observations. North is up, east towards the right-hand side. The 28 fields observed with FLAMES (*outer sample*) are shown as continuous circles. The cluster center and tidal radius (from Trager et al. 1995) are indicated by the black cross and the dashed line, respectively.

temperature transformations by Montegriffo et al. (1998), a reddening $E(B - V) = 0.11$ (Lub 2002) and the extinction coefficients by Savage & Mathis (1979). The gravity parameter $\log g$ has been then computed assuming a distance modulus to ω Cen of $(m - M)_0 = 13.70$ (Bellazzini et al. 2004; Del Principe et al. 2006). The microturbulence velocity has been initially set as 2 Km s^{-1} and then adjusted within a range of about 1 Km s^{-1} by minimizing the trend in the deduced abundances with EWs for Fe I lines. The average error on the derived metallicities is $\sigma_{[Fe/H]} \sim 0.2 \text{ dex}$. The comparison with the metallicity determinations by Johnson et al. (2008) for the 36 stars in common indicates a difference of $\Delta[Fe/H]_{our-J} = -0.21 \pm 0.25$, indicating an acceptable agreement for the purposes of the present study, that is focused on the kinematics in the outer regions of ω Cen. Here we derived metallicities of our stars to have an independent sanity check of the selection criteria adopted in §3 to identify cluster members. A full analysis of the abundance pattern of the selected stars will be the subject of a more detailed dedicated analysis, that will be presented in a forthcoming paper.

3 RADIAL VELOCITY AND METALLICITY DISTRIBUTION

In Figure 3 the radial velocities of the entire sample are plotted as a function of the distance from the cluster center. To calculate distances we deprojected right ascension and declination into X and Y coordinates with the following relations, suited for extended objects that are not close to the celestial equator (from van de Ven et al. 2006):

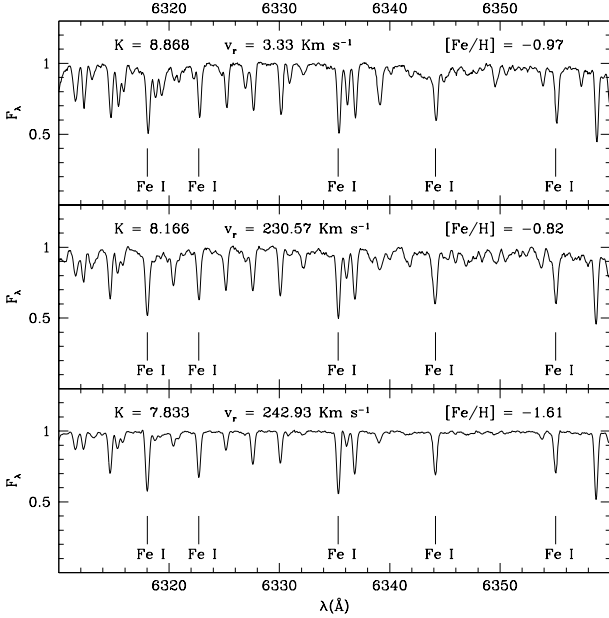


Figure 2. Spectra of the field star 2MASS13331099-4749262 (top panel), and of the ω Cen stars 2MASS13262366-4742424 (middle panel) and 2MASS13283381-4732055 (bottom panel). A sample of iron lines used in the analysis are also indicated.

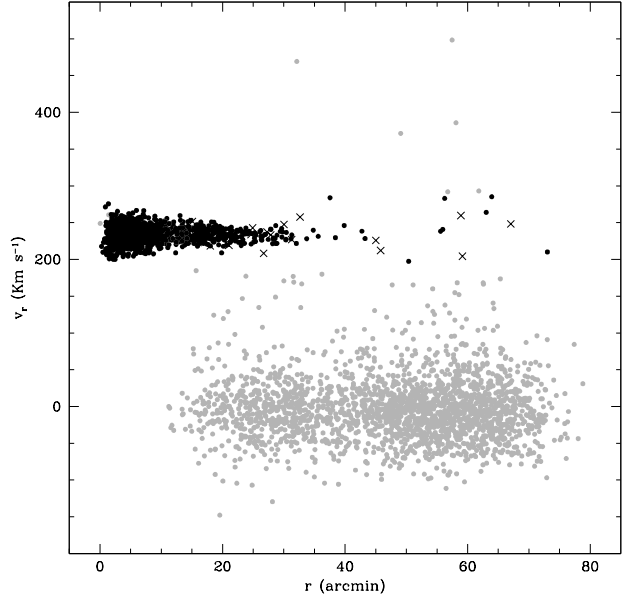


Figure 3. The radial velocities of the entire sample are plotted as a function of the distance from the cluster center. Grey points represent object rejected by the radial velocity selection criterion (i) defined in Sect. 4.1. Crosses represent object rejected by the other selection criteria.

$$X = -r_0 \cos \delta_0 \sin(RA - RA_0)$$

$$Y = r_0 [\sin \delta \cos \delta_0 - \cos \delta \sin \delta_0 \cos(RA - RA_0)]$$

where RA_0 and δ_0 are the coordinate of the cluster center and $r_0 = 10800/\pi$ is the scale factor to have X and Y in arcmin. At the adopted distance, 1 arcmin corresponds to 1.6 pc. As can be noted, the clump of ω Cen stars is clearly visible at large positive velocities ($v_r > 190 \text{ Km s}^{-1}$) while field stars are broadly distributed around the average velocity $\langle v_r \rangle = -8.0 \pm 30.2 \text{ Km s}^{-1}$, in good agreement with the predictions of the Galactic model by Robin et al. (2003; hereafter R03) for thin disc and thick disc stars in this direction, and very different from the typical velocity of ω Cen ($\langle v_r \rangle = 233.2 \pm 0.4 \text{ Km s}^{-1}$).

Figure 4 shows the metallicity distribution obtained for the 338 stars belonging to the *outer sample* and with radial velocity $190 < v_r < 290 \text{ Km s}^{-1}$. A sharp and asymmetric peak at $[Fe/H] \sim -1.8$ can be seen, with a long tail extending toward higher metallicity ($[Fe/H] > -1.4$). Secondary peaks are also visible at metallicity $[Fe/H] \sim -1.3$ and $[Fe/H] \sim -0.85$, in agreement with the previous spectroscopic determinations by Norris et al. (1996), Suntzeff & Kraft (1996) and Johnson et al. (2008).

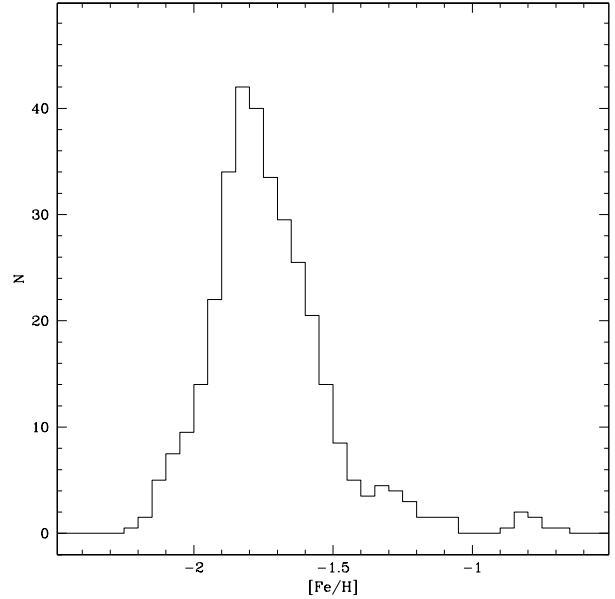


Figure 4. Metallicity distribution of the 338 stars belonging to the *outer sample* with radial velocity $190 < v_r < 290 \text{ Km s}^{-1}$. The distribution is obtained using a running box of 0.1 dex width and a step size of 0.05 dex.

4 VELOCITY DISPERSION

4.1 Selection criteria

In order to construct the velocity dispersion profile of ω Cen we need to distinguish the bona-fide cluster stars from the

Galactic field contamination. In fact, although the field population and ω Cen stars have very different bulk velocities, a small (but non negligible) fraction of stars belonging to the Galactic halo could lie in the same velocity range of genuine cluster stars. This is particularly important in the external region where the cluster density drops quickly with radius, while the density of the field population remains constant (see §6).

To this aim, we excluded from the *inner sample* all the stars with radial velocity $v_r < 190 \text{ Km s}^{-1}$ (see P07) and adopted three different selection criteria for the *outer sample*:

- *i) Radial velocity:* The bulk radial velocity of ω Cen has been estimated to be $\langle v_r \rangle = 233.2 \pm 0.4 \text{ Km s}^{-1}$ with a maximum velocity dispersion at the center of $\sigma_v \simeq 20 \text{ Km s}^{-1}$ (Meylan et al. 1995). Therefore, a first selection has been made by taking as possible members only stars with $190 < v_r < 290 \text{ Km s}^{-1}$ ². Note that this selection is safe since the velocity dispersion is expected to decrease significantly at large distances from the center. Therefore this criterion is not expected to introduce any bias in the selected sample.

- *ii) Position in the CMD:* Figure 5 shows the K vs ($J-K$) CMD of the *outer sample* stars. We considered as cluster members only the stars lying within the selection box enclosing the cluster RGB that we have originally adopted to chose high-priority targets, that is shown in Fig. 5.

- *iii) Proper motions:* We identified 245 stars in common with the proper motion catalog by van Leeuwen et al. (2000). These authors provide for each star a membership probability calculated according to its position in the proper motions plane. On the basis of this additional information, we excluded all the 20 stars with a membership probability smaller than 50%.

A total of 946 stars passed the above selection criteria, 628 belonging to the *inner sample* and 318 belonging to the *outer sample*. In Figure 3 the accepted and rejected stars are clearly indicated. The adopted approach is rather conservative as our aim is to obtain the most reliable sample of cluster members to study the kinematics in the outer regions where the velocity dispersion is low and can be biased by a limited number of spurious sources. On the other hand, while the second and, in particular, the third criterion listed above may exclude from the sample some genuine member, this cannot bias our results as these selections are independent of the radial velocity of the stars. Nevertheless, is interesting to note that using the R03 Galactic model as described in §6, below, we expect a very low degree of contamination. In particular, the predicted number of Galactic stars with $190 < v_r < 290 \text{ Km s}^{-1}$ in our sample is 2.2 ± 0.5 for $r \leq 15'$, 1.4 ± 0.3 for $15' < r \leq 28'$, and 1.4 ± 0.3 in the range $28' < r \leq 44'$ (see §6 for a discussion of the $r > 44'$ region).

Another potential selection criterion is based on the metallicity. Note, however, that only Galactic halo stars are expected to contaminate the sample at velocities

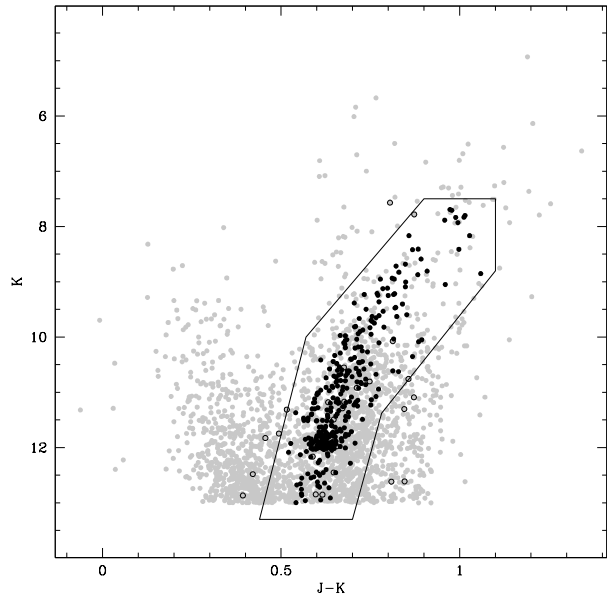


Figure 5. K vs. ($J-K$) CMD of ω Cen. Grey points represent the stars rejected by the radial velocity selection criterion (*i*) defined in Sect. 4.1. Open points represent stars rejected by the other selection criteria. The adopted selection box is also shown. The clump of member stars around $K \simeq 11.7$ is the RGB bump of the cluster (see Sollima et al. 2004).

$190 \text{ Km s}^{-1} < v_r < 290 \text{ Km s}^{-1}$. This Galactic component have a metallicity distribution ranging between $-2.2 < [Fe/H] < -0.8$ with a peak at $[Fe/H] = -1.6$ (Ivezic et al. 2008) Moreover, the contaminating halo stars lie in the foreground and background of ω Cen. Their different distances translate into a wrong determination of their surface gravities and, consequently, spread out their original metallicity distribution. As a consequence, the resulting metallicity distribution of the halo population largely overlaps the metallicity distribution of the ω Cen stars. Therefore, this selection criterion is poorly efficient in discriminating the cluster membership. However, we considered also a sample retaining only the stars whose metallicity is close to the main peak of the metallicity distribution shown in Figure 4 ($-1.95 < [Fe/H] < -1.55$). In the following paragraph we calculated the velocity dispersion profile of ω Cen with and without adopting this last criterion, as a further check of our results.

4.2 Method

Once selected the bona-fide cluster member stars, as a first step we corrected for perspective rotation. In fact, since ω Cen has a large extension on the plane of the sky (with a diameter about twice that of the full moon), its systemic motion produces a non-negligible amount of apparent rotation (Feast 1961). We corrected for this effect using the following correction (see van de Ven et al. 2006):

$$\Delta v_r = 0.001379 (X\mu_X + Y\mu_Y) D \text{ Km s}^{-1}$$

to be subtracted to the observed v_r . $\mu_X = 3.88$ and

² The choice of an asymmetric range has been performed to minimize the field contamination in the region where the bulk of the field stars are located.

$\mu_Y = -4.44$ are the systemic proper motions in units of $mas\ yr^{-1}$ (van Leeuwen 2000) and $D = 5.5$ is the distance to ω Cen in kpc (Bellazzini et al. 2004; Del Principe et al. 2006).

As a second step, we divided the sampled area in a set of concentric annuli at various distances from the cluster center, searching for the best compromise to have well populated and compact radial bins (except for the innermost $r < 1'$ bin that is not relevant in this context). Within each annulus we calculated the value of σ_v that maximize the log-likelihood

$$L(\sigma_v) = \sum_{i=1}^N \log \int_{-\infty}^{+\infty} \frac{e^{-\frac{(v_i - \langle v \rangle)^2}{2\sigma_v^2}} e^{-\frac{(v_i - \langle v \rangle)^2}{2\sigma_i^2}}}{2\pi \sigma_v \sigma_i} dv$$

where v_i and σ_i are the radial velocity and its corresponding error for the N stars contained in the annulus and $\langle v \rangle$ the average cluster velocity (Walker et al. 2006). As a further selection, in each annulus we excluded the outliers stars whose radial velocity differs more than 3 times the *local* σ_v from the cluster bulk velocity (see Figure 6; Bellazzini et al. 2008).

The derived velocity dispersion profile is listed in Table 1 and shown in Figure 7 for the case of the sample selected with (filled points) and without (open points) the metallicity selection criterion. As can be noted, no significant differences are evident between the two profiles. For this reason, in the following we refer always to the sample not selected in metallicity. The obtained profile shows a central velocity dispersion of $\sigma_v = 17.2^{+4.6}_{-3.0} Km\ s^{-1}$ in agreement with the previous estimates by Meylan et al. (1995), Mayor et al. (1997) Norris et al. (1997) and van de Ven et al. (2006). The measured velocity dispersion appears to decrease monotonically with distance out to $r \simeq 26'$ from the cluster center, where it reaches a minimum of $\sigma_v = 5.2^{+0.80}_{-0.65} Km\ s^{-1}$. A small, non statistically significant, increase of the velocity dispersion is noticeable in the last bin, at a distance of $\sim 32'$.

In Figure 8 the obtained velocity dispersion profile is compared with the profiles obtained by van de Ven et al. (2006) and Scarpa et al. (2003). Note that our profile agree very well with that obtained by van de Ven et al. (2006) in the overlapping region $r \leq 20'$. At distances $r > 24'$ the behaviour of our profile differs from that obtained by Scarpa et al. (2003). In particular, while the profile by Scarpa et al. (2003) flattens around a value of $\sigma_v \sim 8 Km\ s^{-1}$, our profile continues to decrease. The statistical disagreement between the two profiles is $\sim 2\sigma$, hence it cannot be considered as statistically significant. The number of target stars in range $20' \lesssim r \lesssim 28'$ and the accuracy of the radial velocity estimates of the present study is similar to Scarpa et al. (2003). However, Scarpa et al. (2003) do not report (a) if their velocities have been corrected for perspective rotation (§4.2) and (b) the details of the adopted selection criteria; in particular it is not said if the selection in v_r takes into account the *local* value of the velocity dispersion at the considered radius. In any case, our results indicate that the flattening of the velocity dispersion curve shown by Scarpa et al. (2003) may not reflect a real kinematic feature of the cluster but a chance fluctuation, instead. The (doubtful) increase of the dispersion in the $\langle r \rangle \simeq 32'$ bin observed here, if real, would be more compatible with the onset of tidal heating that with

Table 1. Velocity dispersion profile of ω Cen.

r	$\langle r \rangle$	N	σ_v	$\Delta \sigma_v$
arcmin	arcmin		Kms^{-1}	Kms^{-1}
0 - 1	0.75	10	17.20	+4.60 -3.00
1 - 2	1.51	50	16.66	+1.80 -1.50
2 - 3	2.50	80	15.16	+1.30 -1.10
3 - 4	3.49	91	14.32	+1.20 -0.95
4 - 6	5.04	151	13.34	+0.80 -0.70
6 - 8	6.99	112	12.17	+0.85 -0.80
8 - 12	9.63	150	10.15	+0.60 -0.60
12 - 16	14.01	98	9.19	+0.70 -0.60
16 - 20	17.75	99	8.28	+0.65 -0.55
20 - 24	21.79	48	6.39	+0.70 -0.55
24 - 28	25.71	24	5.21	+0.80 -0.65
28 - 44	32.25	26	7.01	+1.10 -0.90

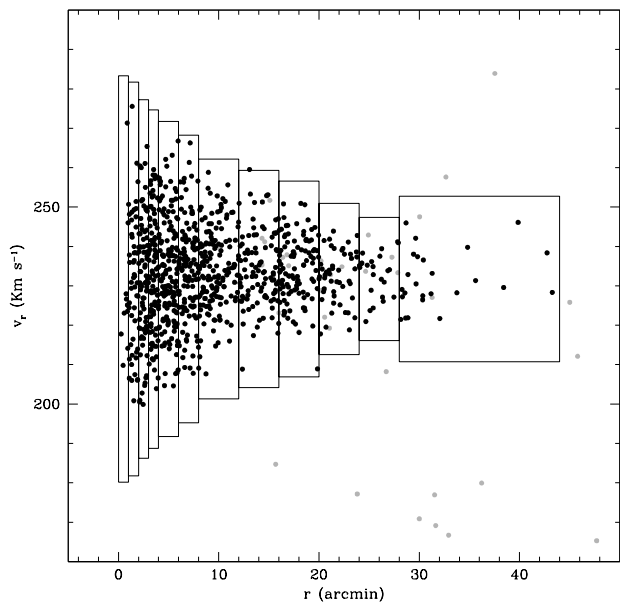


Figure 6. Radial velocity distribution as a function of the distance from the cluster center for stars with $190 < v_r < 290 Km\ s^{-1}$. The adopted bins of variable size are indicated together with the local 3σ range. Grey points represent the object rejected by the selection criteria defined in Sect. 4.1

the effects of MOND or DM (see §5.2; see also Muñoz et al. 2008, and references therein). Note that this last bin is located outside the radial range covered by Scarpa et al.'s data.

5 COMPARISON WITH THEORETICAL MODELS

To check if canonical dynamical models are able to reproduce the observed kinematics of ω Cen, in the following sections we compare our data with a set of analytical models (Wilson 1975). N-body simulations have also been per-

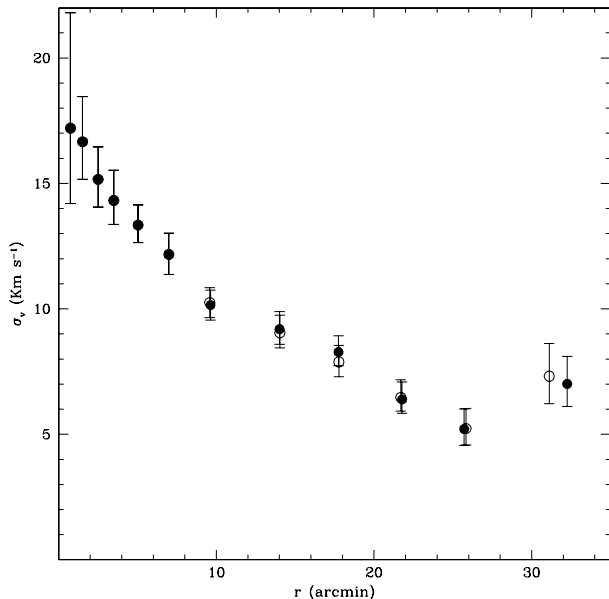


Figure 7. Velocity dispersion profile of ω Cen. Open and filled points refers to the sample selected and not selected in metallicity, respectively.

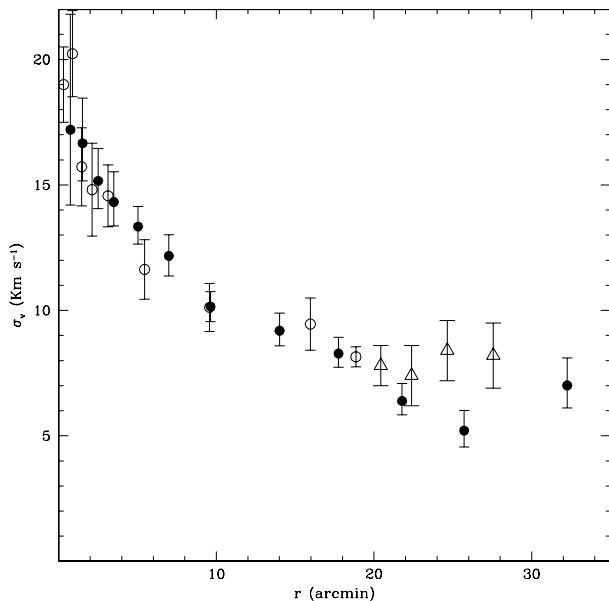


Figure 8. Comparison between the velocity dispersion profile presented in this paper (filled points) with those by van de Ven et al. (2006; open points) and by Scarpa et al. (2003; open triangles).

formed to study the effects of the tidal field of the Milky Way on different models of the cluster.

5.1 Analytical models

We attempt to reproduce our observations using Wilson (1975) models. These models have the advantage of taking into account the cluster rotation, predicting simultaneously the surface brightness, the velocity dispersion, the rotation, and the ellipticity profiles. These models adopt the distribution function

$$f(E, J) = \begin{cases} (e^{-E} - 1 + E)e^{\beta J - \frac{1}{2}\zeta^2 J^2} & \text{if } E < 0 \\ 0 & \text{if } E \geq 0 \end{cases}$$

Any choice of the a -dimensional central potential U_0 , and of the two free parameters of the above equation (β and ζ), yields a different rotating model in virial equilibrium. The adoption of a core radius r_c and of the inclination angle respect to the plane of the sky i provide an actual realization of the model that can be compared with observations. We explored the parameter space to find out one set reproducing simultaneously *i*) the surface brightness profile, *ii*) the velocity dispersion profile, *iii*) the rotation curve and *iv*) the ellipticity profile, giving lower weight to this last item. We adopt the velocity dispersion profile derived in Sect. 4.2, the surface brightness profile by Trager, King & Djorgovski (1995) and the ellipticity profile by Geyer, Nelles & Hopp (1983). Since the angle of rotation in the plane of the sky of ω Cen is $\phi \sim 0^\circ$, the rotation curve corresponds to the $X - v_r$ diagram.

The best-fit model has been found by fixing the inclination angle $i = 48^\circ$ (van de Ven et al. 2006) and assuming $U_0 = -6.3$, $\beta = 0.8$, $\zeta = 0.4$ and $r_c = 2.8'$. The ratio between the rotational kinetic energy and the absolute value of the potential energy of this model is $T/|W| = 0.09$, indicating that it is stable against non-axisymmetric perturbations (Ostriker & Peebles 1973). The fit of the observational data with this model is shown in Figure 9. As can be noted, the agreement is good in all the four diagrams. In particular, the model well reproduces all the observed kinematic properties of the cluster (rotation and dispersion) over the entire radial range covered by our data³. This means that *the velocity dispersion and rotation profiles of ω Cen are fully consistent with an equilibrium model in which the mass distribution follows the light, in the framework of classical Newtonian gravitation.* This is in good agreement with the results by McLaughlin & Meylan (2003), that were limited to the velocity dispersion profile.

5.2 N-body simulations

As described in Sect. 1, there is no strong evidence for the presence of a significant population of tidally stripped stars around ω Cen. The most thorough study in this sense is the one by Da Costa & Coleman (2008) that, from their extensive radial velocity survey, concluded that less than 0.7%

³ The marginal disagreement between the predicted and observed velocity dispersion profile in the innermost region could be induced by many second-order effects in modelling the shape of the velocity distribution in the internal cluster region (e.g. non-rotational anisotropy) and/or by the possible presence of an intermediate-mass black hole object in the center of ω Cen (as proposed by Noyola, Gebhardt & Bergmann 2008)

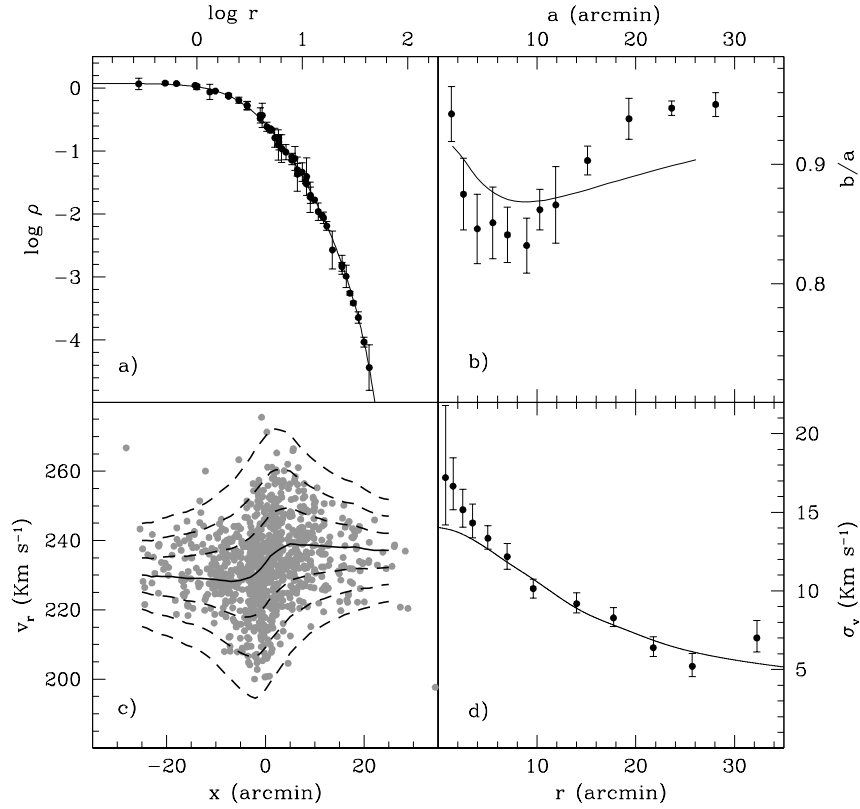


Figure 9. Comparison between the best-fit Wilson (1975) model (solid lines) and a) the projected surface brightness (from Trager et al. 1995) b) the ellipticity profile (from Geyer et al. 1983) c) the rotation curve and d) the velocity dispersion profile presented in this paper. In panel c) the 1σ , 2σ and 3σ contours predicted by the model are also shown as dashed lines.

of the total cluster mass is comprised between 1 and 2 tidal radii. This result implies that the stripping process must have been largely completed at early epochs. Therefore, if ω Cen is indeed the remnant of a larger system destroyed long time ago, it must have lost a large part of its stars in a orbit with a larger apogalacticon with respect to the present day, because of orbital decay due to dynamical friction (Zhao 2002; Bekki & Freeman 2003; see also Tsuchiya et al. 2004; Mizutani et al. 2003 and Ideta & Makino 2004). This implies that the present-day system should be approximately in equilibrium with the tidal field of the Milky Way and lie on a stable orbit, as its mass is now sufficiently low to make the effect of dynamical friction negligible.

We adopt this view as a working hypothesis for a simple N-body simulation aimed at studying the spatial distribution and the kinematical properties of the stars eventually stripped from the cluster by the tidal field of the Galaxy while the system is in the present-day stable orbit (see Ideta & Makino 2004). The very good knowledge of the distance and 3-D motion of ω Cen (van Leeuwen 2000) gives a high predictive power, under the limitations of the assumed hypothesis. For more detailed and extensive studies see Bekki & Freeman (2003), Tsuchiya et al. (2004), Ideta & Makino (2004), and references therein.

The simulation was performed with `falcON`, a fast

and momentum-conserving tree-code (Dehnen 2000, 2002), within the NEMO environment (Tauben 1995). Gravity was softened with the kernel ‘ P_2 ’ of Dehnen (2000), with a softening length of 2 pc. The model cluster was let to evolve within the three-component (bulge+disc+halo) static Galactic potential 2b of Dehnen & Binney (1998), which has $v_{rot}(R_\odot) = 231 \text{ Km s}^{-1}$ and a total mass within 100 kpc of $\simeq 1 \times 10^{12} M_\odot$. ω Cen was represented by 50000 particles distributed according to an equilibrium King (1966) model having $W_0 = 6.0$, $r_t = 100 \text{ pc}$ and $M = 5 \times 10^6 M_\odot$. This model has concentration (c) and tidal radius (r_t) values similar to the real cluster; the central velocity dispersion is also very similar, $\sigma \simeq 17.0 \text{ Km s}^{-1}$, but it should be recalled that the initial velocity distribution is completely isotropic, lacking any intrinsic rotation. `falcON` is best suited to follow the evolution of non-collisional systems. While the effects of two-body encounters have been shown to be negligible in ω Cen (Ferraro et al. 2006; Sollima et al. 2007), this may not be the case in the innermost region of our model. To minimize undesired effects due to two-body encounters in the densest part of the model we have adopted a softening length approximately as large as the cluster core radius. For this reason the evolution in the innermost few r_c of the model should not be considered as a good representation of the evolution of the real cluster. On the other hand our

model is fully adequate to study the reaction of the outer regions to the tidal strain of the Galactic potential, i.e. the morphology and the kinematics of possible tidal tails, that is what we are interested into. Note also that the 2-body relaxation time at the half-mass radius of our model (Binney & Tremaine 1998, their Eq. 4-9) is a factor of $\simeq 4$ larger than the duration of our simulation, hence, in any case, the effects of particle encounters on the global properties of the model should be negligible.

First of all we integrated backward in time, within the adopted potential, the orbit of a test particle whose initial position and 3-D velocity coincide with those of ω Cen at the present epoch (position from Bellazzini et al. 2004 and velocity from van Leeuwen et al. 2000). The orbit has a period of $\simeq 80$ Myr, pericentric and apocentric distances of 1.5 kpc and 6.5 kpc, respectively, very similar to the orbits derived by Mizutani et al. (2003) and Ideta & Makino (2004). We launched our $N=50000$ particle model from the apocenter at the epoch $t=0.972$ Gyr in the past. With this assumption the cluster evolves within the adopted potential for more than 10 orbits from that time to the present epoch ($t=0$). At the end of the simulation the model is within 40 pc of the current position of ω Cen, and the 3-D velocity is within 5% of the real cluster velocity. The distribution of the particles at the end of the simulation (see Fig. 10) is in good agreement with the results by Ideta & Makino (2004) and Mizutani et al. (2003). The remnant have developed two tidal tails extending over the whole orbital path. However, the tidal radius of the bound remnant is only 10% smaller than the initial model and there is a mere 8% of the particles that lie outside that radius after 10 perigalactic passages. This confirms that ω Cen is currently nearly at equilibrium with the tidal field of the Milky Way and that any tidal tail originating from the present day cluster should be very weak and hard to detect. In particular, it is interesting to note that only 0.4% of the particles are found in the annulus between $1 r_t$ and $2 r_t$, in excellent agreement with the results of Da Costa & Coleman (2008). Rescaling to the observed total luminosity of the cluster the average surface brightness in that annulus due to tidally stripped stars is $\mu_V \sim 30.0$ mag/arcsec².

In Figure 11 the final surface brightness and the velocity dispersion profiles of the simulated satellite are shown. As can be noted, the surface brightness profile deviates from the King profile at $r > 40'$, following the power-law trend typical of tidally stripped stars (see Johnston, Sigurdsson & Hernquist 1999; Muñoz et al. 2008, and references therein). This deviation occurs at a very low surface density level (about 3.5 orders of magnitude lower than the center), just outside the limit reached so far by any photometric investigation. Note that neither King models nor Wilson's ones can reproduce this external behaviour.

Also the velocity dispersion profile shows a departure from the predicted King profile. However, in this case the drift already occurs at $r \sim 25'$ yielding a flatter profile at larger distances. In any case, the derived profile is compatible with the observed one, within the uncertainties. Hence, the available observations appear still compatible with the tidal stripping scenario described by our N-body model. Fig. 11 suggests that the "easiest" way to look for the observational signatures of the ongoing formation of tidal tails would be to reliably extend the surface brightness profile

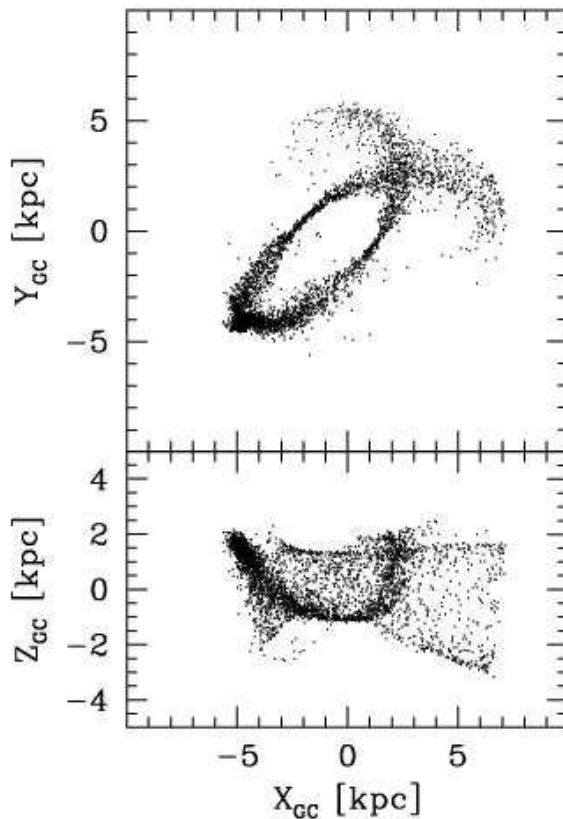


Figure 10. Position of the particles at the end of the N-body simulation A (present epoch) in galactocentric coordinates. The X-Y plane coincides with the Galactic Plane, the X-Z plane is perpendicular to it and passes through the Sun. Note the excellent agreement with the much finer simulation by Ideta & Makino (2004; the upper right panel of their Fig. 2).

using abundant and easy-to-select tracers as Main Sequence stars, searching for the power-law branch of the profile.

6 THE OUTER REGION

In Sect. 4 we presented the velocity dispersion profile of ω Cen calculated out to a distance of ~ 32 arcmin, and comprising stars out to $r = 44'$ from the cluster center. A more careful analysis is needed when considering the region at $r > 44'$ i.e. close to the cluster tidal radius. In this region, only seven stars passed the selection criteria defined in Sect. 4.1. The resulting velocity dispersion of this sample is $\sigma_v = 36.0^{+12.5}_{-7.5}$ Km s⁻¹, about a factor of 2 larger than the central value, and a factor of 5 larger than the outermost point of the profile, at $\langle r \rangle \simeq 32$. It is worth noticing that although the adopted selection criteria are efficient in eliminating the contaminating field stars in the inner region of the system, their efficiency decrease at larger distances, as the surface density of ω Cen stars plunges below the background level due to Galactic field stars.

To check the membership of these sample of stars we performed various tests. First, we compared our sample with the predictions of the R03 Galactic model. Although this model is only a statistical representation of the Galactic field population (see Drimmmel et al. 2005), it gives a good

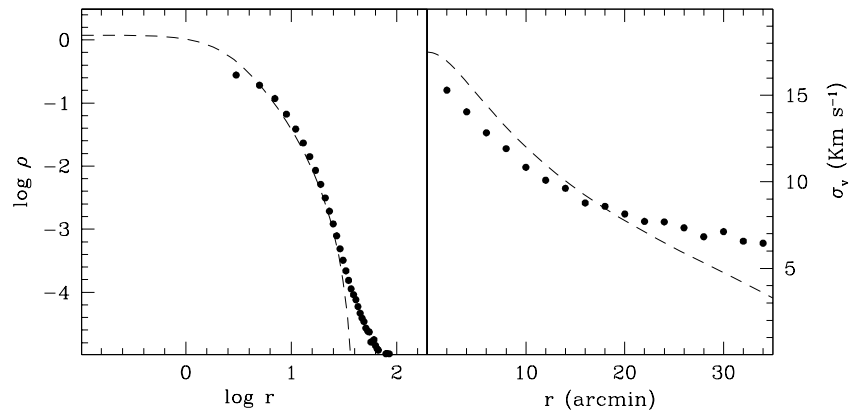


Figure 11. Surface brightness (left panel) and velocity dispersion (right panel) profiles for the bound remnant at the end of the N-body simulation A (filled circles). The dashed lines are from the King (1966) model that best fits the final surface brightness profile.

estimate of the order of magnitude of the field contamination. To minimize the effect due to small number statistics, we retrieved (and merged together) two simulated catalogue covering an area of 5 square degrees each, in the direction of ω Cen. The v_r distributions of simulated stars approximately lying in the same magnitude and colour range of the observed stars is well fitted by a sum of two Gaussian distributions, one for the main peak of thin disc + thick disc Galactic stars at $-150 < v_r < 150 \text{ Km s}^{-1}$, the other for the Halo population. Once fixed the density normalization of the two components, the number of stars expected in our sample, in any given range of r and v_r is easily obtained by re-normalizing the Gaussian of the main component to the number of observed stars having $-150 < v_r < 150 \text{ Km s}^{-1}$ in that range. Adopting this procedure, the expected number of field stars with $190 < v_r < 290 \text{ Km s}^{-1}$ at distances $r > 44'$ turns out to be $N_{field} = 4.0 \pm 0.9$. Therefore, according to this test, about half of the outermost stars are likely non-members, Galactic Halo stars.

Another possibility is to estimate the number of cluster stars expected at such distance by means of the cluster density profile. Indeed, in a given radial bin (defined between r_1 and r_2) the expected ratio between the number of cluster stars (N_{mem}) and field stars (N_{field}) can be written as

$$\frac{N_{mem}}{N_{field}} = \frac{\int_{r_1}^{r_2} 2\pi r \rho_{mem} dr}{\int_{r_1}^{r_2} 2\pi r \rho_{field} dr} = C \frac{\int_{r_1}^{r_2} r \rho_{mem} dr}{\int_{r_1}^{r_2} r dr} \quad (1)$$

where ρ_{mem} and ρ_{field} represent the projected surface density of member stars and field stars, respectively. In the above equation the density of field stars has been assumed to be constant over the field of view of the cluster. We counted N_{field} as the number of stars with $190 \text{ Km s}^{-1} < v_r < 290 \text{ Km s}^{-1}$ in each radial bin and estimated the constant C by best-fitting the ratio N_{mem}/N_{field} measured in the innermost bins (at $r < 44'$) with the prediction of the best-fit Wilson (1975) model described in Sect. 5.1. Then, we estimated the number of cluster members stars in the most external bin by using eq. 1 and N_{field} measured in this bin. Following this procedure we estimated $N_{mem} = 0.4$ at

$r > 44'$. However, as shown in Sect. 5.2, the interaction between ω Cen and the Milky Way would produce a departure from the King profile in the external region of the cluster, implying a higher surface density. Therefore, the number of cluster members stars in the external region is expected to be larger than this estimate. We performed the above procedure also assuming at $r > 40'$ a power-law density profile with index $\alpha = -3.8$ (i.e. the slope predicted by our N-body simulation). Also in this case, the expected number of cluster members results $N_{mem} = 1.5$. Thus, according to this test, the majority of the high-velocity external stars should be field stars.

It is interesting to note that none of the seven considered stars pass the metallicity selection criterion defined in Sect. 4.1. A Kolmogorov-Smirnov test gives a probability smaller than 0.2% that the metallicity of these stars can be randomly extracted from the metallicity distribution of the entire sample of cluster members stars shown in Figure 4. Given all the result above we can safely conclude that most of (if not all) the seven stars passing our selection criteria at $r > 44'$ are likely not member of the cluster.

Having established that, we draw the attention of the reader on a curious occurrence. In Figure 12 the radial velocities of the stars with $190 < v_r < 290 \text{ Km s}^{-1}$ is shown as a function of the right ascension for the observed sample and for the particles of the N-body model described in Sect. 5.2. Note that the most external stars are not evenly distributed in the considered plane. Most of the $r > 44'$ stars lying to the West of the cluster have v_r larger than the systemic cluster velocity, while the opposite is true for $r > 44'$ Eastern stars. This apparent trend of mean v_r with RA is in the same sense as that expected to be imprinted by the Galactic tidal field on stripped stars, clearly visible in the N-body model (lower panel of Fig. 12). By means of Monte-Carlo extractions from the synthetic R03 catalogue described above, we estimated that the chance occurrence of such an asymmetry in Halo stars is lower than 5%. If the observed gradient would be revealed as real using a much larger sample of stars in this range of distances, this would

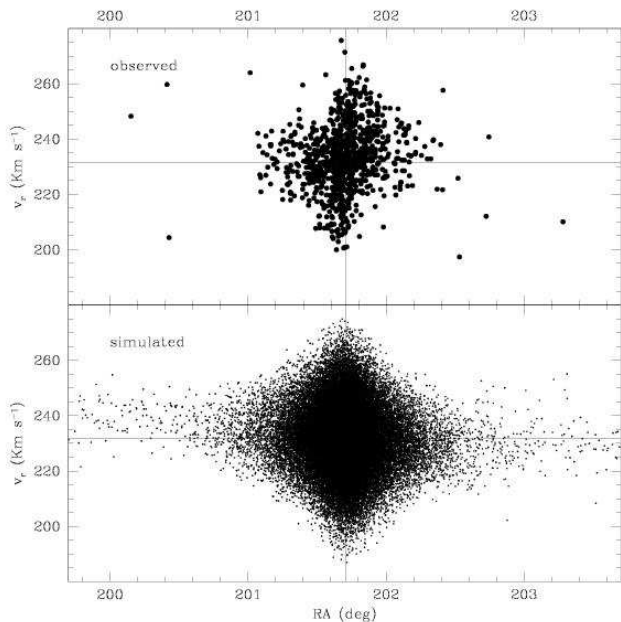


Figure 12. The radial velocities of the stars with $190 < v_r < 290 \text{ Km s}^{-1}$ is shown as a function of the right ascension for the observed sample (top panel) and for the N-body simulation described in Sect. 5.2 (bottom panel).

make very difficult to interpret most of these stars as belonging to the Galactic Halo and the hypothesis of a tidal tail must be reconsidered. Another interesting issue emerges from this comparison: in the innermost region of the cluster ($201.0^\circ \lesssim RA \lesssim 202.3^\circ$ in Fig12), the clear S-shaped trend due to the cluster rotation is clearly visible. In particular, in this case the Eastern branch of the rotation curve has larger average v_r with respect to the Western branch. This trend is just in the opposite direction of what produced in the N-body simulation by the Galactic tidal strain. This strongly suggest that the rotation in the inner $30'$ of ω Cen is not induced the interaction with the Milky Way, as previously suggested by van de Ven et al. (2006), but it is an intrinsic property of the system, instead.

7 SUMMARY AND CONCLUSIONS

In this paper we present high accuracy radial velocities for a sample of more than 2500 stars in the direction of ω Cen. Adding the homogeneous sample by P07 and applying various un-biased selection criteria, we selected a sample of 946 bona-fide cluster's members displaced over a wide region up to a distance of $\sim 80'$ from the cluster center.

We derived a very reliable velocity dispersion profile in the range $1.5' \leq r \leq 28'$. In this range the velocity dispersion appears to decrease monotonically from a central value of $\sigma_v \sim 17.2 \text{ Km s}^{-1}$ down to a minimum value of $\sigma_v \sim 5.2 \text{ Km s}^{-1}$. A non-statistically significant raise to $\sigma_v \simeq 7.0 \pm 1.0 \text{ Km s}^{-1}$ is observed in an outer extended radial bin ($28' \leq r < 44'$), that must be considered with great caution because of the uneven radial distribution of the 26 candidate member stars included. The obtained profile is

consistent with those obtained by previous authors within $r \simeq 20'$ (Meylan et al. 1995; Mayor et al. 1997; van de Ven et al. 2006) but differs from that derived by Scarpa et al. (2003) in the most external region of the cluster. In particular, at odds with the Scarpa et al.'s analysis, we did not find any sign of flattening of the velocity dispersion profile in the region between $20' < r < 28'$.

The observed velocity dispersion profile of ω Cen, as well as its structural and kinematical properties is well reproduced by a Wilson (1975) equilibrium model in which mass follows light. Therefore, with the present data we find no evidences of neither the presence of dark matter nor MOND effects, at least in the inner $30'$ from the center.

The majority of the seven candidate members we found at $r > 44'$ are consistent with being iterlopers from the Galactic Halo. The only piece of evidence that is in marginal contrast with this view is that they seem to display a velocity gradient similar to that expected for star tidally stripped from ω Cen, according to the prediction of a simple N-body model. The comparison with the same N-body model suggest that the well-known rotation pattern observed in the inner $30'$ of ω Cen is not produced by the Galactic tidal strain, but it should be intrinsic to the stellar system, instead.

The present study, mainly focused on the kinematics in the range $20' \lesssim r \lesssim 30'$, as well as that performed by Da Costa and Coleman (2008), focused on the search of extra-tidal stars ($60' \lesssim r \lesssim 120'$), reached the limits that can be achieved using RGB stars as tracers. Future studies aimed at assessing the shape of the velocity dispersion profile in the range $30' \lesssim r \lesssim 60'$ and trying to identify extra-tidal stars must rely on much more abundant Main Sequence stars.

ACKNOWLEDGMENTS

This research was supported by the Instituto de Astrofísica de Canarias. M.B., M.C., E.P., and R.S. acknowledge the financial support to this research by INAF through the PRIN-2007 Grant CRA 1.06.10.04. We warmly thank Paolo Montegriffo for assistance in the analysis. We also thank the anonymous referee for his helpful comments and suggestions.

REFERENCES

- Bekki K., Freeman K.C., 2003, MNRAS, 346, L11
- Bellazzini M., Ferraro F. R., Sollima A., Pancino E., Origlia L., 2004, A&A, 424, 199
- Bellazzini M. Ibata R.A., Chapman S.C., Mackey A.D., Monaco L., Irwin M.J., Martin N.F., Lewis G.F., Dallengandro E., 2008, AJ, 136, 1147
- Baumgardt H., Grebel E.K., Kroupa P., 2005, MNRAS, 359, L1
- Binney, J., Tremaine, S., Galactic Dynamics, Princeton, Princeton University Press
- Carraro G., Lia C., 2000, A&A, 357, 977
- Combes, F., Leon, S., Meylan, G., 1999, A&A, 352, 149
- Da Costa G. S., Coleman M. G., 2008, AJ, 136, 506
- Dehnen W., Binney J., 1998, MNRAS, 294, 429
- Dehnen, W., 2000, ApJ, 536, L39
- Dehnen, W., 2002, J. Comput. Phys, 179, 27

- Del Principe M., et al., 2006, *ApJ*, 652, 362
- Dinescu D. I., Girard T. M., van Altena W. F., 1999, *AJ*, 117, 1792
- Dinescu D. I., 2002, in "Omega Centauri, A Unique Window into Astrophysics", *ASP Conf. Ser.*, 265, 365
- Drimmel R., Bucciarelli B., Lattanzi M. G., Spagna A., Jordi C., Robin A. C., Reylé C., Luri X., 2005, in "The Three-Dimensional Universe with Gaia", 576, 163
- Feast M. W., 1961, *MNRAS*, 122, 1
- Federici L., Bellazzini M., Galletti S., Fusi Pecci F., Buzzoni A., Parmeggiani G., 2007, *A&A*, 473, 429
- Ferraro, F. R., Sollima, A., Rood, R. T., Origlia, L., Pancino, E., Bellazzini, M., 2006, *ApJ*, 638, 433
- Freeman K. C., 1993, in "The Globular Cluster-Galaxy Connection", *ASP Conf. Ser.*, 48, 608
- Freeman K. C., Rodgers A. W., 1975, *ApJ*, 201, L71
- Geyer E. H., Nelles B., Hopp U., 1983, *A&A*, 125, 359
- Gilmore, G., Wilkinson, M.I., Wyse, R.F.G., Kleya, J.T., Koch, A., Wyn Evans, N., Grebel, E.K., 2007, *ApJ*, 663, 948
- Haghi H., Baumgardt H., Kroupa P., Grebel E.K., Hilker M., Jordi K., 2009, *MNRAS*, in press (arXiv:0902.1846)
- Ideta M., Makino J., 2004, *ApJ*, 616, L107
- Ivezić Ž., et al., 2008, *ApJ*, 684, 287
- Johnson C. I., Pilachowski C. A., Simmerer J., Schwenk D., 2008, *ApJ*, 681, 1505
- Johnston K.V., Sigurdsson S., Hernquist L., 1999, *MNRAS*, 302, 771
- King, I.R., 1966, *AJ*, 71, 64
- Kurucz R. L., 1979, *ApJS*, 40, 1
- Kurucz R. L., Bell R., 1975, Kurucz CD-ROM No. 23 Cambridge, Smithsonian Astrophysical Observatory
- Law D. R., Majewski S. R., Skrutskie M. F., Carpenter J. M., Ayub H. F., 2003, *AJ*, 126, 1871
- Leon S., Meylan G., Combes F., 2000, *A&A*, 359, 907
- Lub J., 2002, in "Omega Centauri, A Unique Window into Astrophysics", *ASP Conf. Ser.*, 265, 95
- Mackey A. D., van den Bergh S., 2005, *MNRAS*, 360, 631
- Mashchenko S., Sills A., 2005, *ApJ*, 619, 243
- Mayor M., et al., 1997, *AJ*, 114, 1087
- McLaughlin D. E., Meylan G., 2003, in "New Horizons in Globular Cluster Astronomy", *ASP Conf. Ser.*, 296, 153
- Merritt D., Meylan G., Mayor M., 1997, *AJ*, 114, 1074
- Meylan G., 1987, *A&A*, 184, 144
- Meylan G., Mayor M., 1986, *A&A*, 166, 122
- Meylan G., Mayor M., Duquenois A., Dubath P., 1995, *A&A*, 303, 761
- Milgrom M., 1983, *ApJ*, 270, 365
- Milgrom M., 2008, in Matter and energy in the Universe: from nucleosynthesis to cosmology, XIX Rencontres de Blois, in press (arXiv:0801.3133)
- Mizutani A., Chiba M., Sakamoto T., 2003, *ApJ*, 589, L89
- Moffat J.W., Toth V.T., 2008, *ApJ*, 680, 1158
- Montegriffo P., Ferraro F. R., Origlia L., Fusi Pecci F., 1998, *MNRAS*, 297, 872
- Moultaka J., Ilovaisky S. A., Prugniel P., Soubiran C., 2004, *PASP*, 116, 693
- Muñoz R. R., Majewski S. R., Johnston K. V., 2008, *ApJ*, 679, 346
- Norris J. E., 2004, *ApJ*, 612, L25
- Norris J. E., Freeman K. C., Mighell K. J., 1996, *ApJ*, 462, 241
- Norris J. E., Freeman K. C., Mayor M., Seitzer P., 1997, *ApJ*, 487, L187
- Noyola E., Gebhardt K., Bergmann M., 2008, *ApJ*, 676, 1008
- Ostriker J. P., Peebles P. J. E., 1973, *ApJ*, 186, 467
- Pancino E., Ferraro F. R., Bellazzini M., Piotto G., Zoccali M., 2000, *ApJ*, 534, L83
- Pancino E., Galfo A., Ferraro F. R., Bellazzini M., 2007, *ApJ*, 661, L155
- Pasquini L., et al., 2002, *The Messenger*, 110, 1
- Piotto G., et al., 2005, *ApJ*, 621, 777
- Reijns R. A., Seitzer P., Arnold R., Freeman K. C., Ingerson T., van den Bosch R. C. E., van de Ven G., de Zeeuw P. T., 2006, *A&A*, 445, 503
- Robin A. C., Reylé C., Derrière S., Picaud S., 2003, *A&A*, 409, 523
- Savage B. D., Mathis J. S., 1979, *ARA&A*, 17, 73
- Scarpa R., Marconi G., Gilmozzi R., 2003, *A&A*, 405, L15
- Scarpa R., Marconi G., Gilmozzi R., Carraro, G., 2007, *The Messenger*, 128, 41
- Skrutskie M. F., et al., 2006, *AJ*, 131, 1163
- Snedden C., 1973, *ApJ*, 184, 839
- Sollima A., Ferraro F. R., Bellazzini M., 2007, *MNRAS*, 381, 1575
- Sollima A., Ferraro F. R., Origlia L., Pancino E., Bellazzini M., 2004, *A&A*, 420, 173
- Suntzeff N. B., Kraft R. P., 1996, *AJ*, 111, 1913
- Teuben P.J., 1995, in *Astronomical Data Analysis Software and Systems IV*, R. Shaw, H.E. Payne nad J.J., Hayes Eds., *ASP Conf. Ser.*, 77, 398
- Trager S. C., King I. R., Djorgovski S., 1995, *AJ*, 109, 218
- Tsuchiya T., Korchagin V. I., Dinescu D. I., 2004, *MNRAS*, 350, 1141
- van de Ven G., van den Bosch R. C. E., Verolme E. K., de Zeeuw P. T., 2006, *A&A*, 445, 513
- van Leeuwen F., Le Poole R. S., Reijns R. A., Freeman K. C., de Zeeuw P. T., 2000, *A&A*, 360, 472
- Walker M.G., Mateo M., Olszewski E.W, Bernstein R., Wang X., Woodroffe M., 2006, *AJ*, 131, 2114
- Wilson C. P., 1975, *AJ*, 80, 175
- Zacharias N., Urban S. E., Zacharias M. I., Wycoff G. L., Hall D. M., Monet D. G., Rafferty T. J., 2004, *AJ*, 127, 3043
- Zhao, H.-S., 2002, in *Omega Centauri: A Unique Window into Astrophysics*, F. van Leeuwen, J.D., Hughes and G. Piotto Eds., *ASP Conf. Ser.*, 265, 391

This paper has been typeset from a \TeX / \LaTeX file prepared by the author.